IET Generation, Transmission & Distribution

Research Article

IET Journals
The Institution of Engineering and Technology

Voltage stability assessment based on improved coupled single-port method

ISSN 1751-8687
Received on 18th December 2016
Revised 17th April 2017
Accepted on 2nd May 2017
doi: 10.1049/iet-gtd.2016.2067
www.ietdl.org

Q1 *Bai Cui[1], Zhaoyu Wang[2]* ✉

[1]*School of Electrical and Computer Engineering, Georgia Institute of Technology, Atlanta, GA 30332, USA*
[2]*Department of Electrical and Computer Engineering, Iowa State University, Ames, IA 50011, USA*
✉ *E-mail: wzy@iastate.edu*

Abstract: This study proposes an improved coupled single-port method for the assessment of voltage stability based on phasor measurement unit (PMU) data. The impedance matching condition, i.e. the condition that the local load impedance and the Thévenin equivalent impedance are equal in magnitude at the loadability limit point, has been a fundamental assumption of many existing studies on voltage stability assessment. However, it is shown in this study that the impedance matching can happen either before or after the loadability limit point in certain cases. The authors have proven that the inaccuracy of the conventional impedance matching condition is due to the time-varying equivalent parameters of a power system. To deal with the dynamic nature of grid equivalence, they propose an innovative method to improve the conventional coupled single-port method. In the new method, voltage magnitude-to-load consumption sensitivity is used to adjust the equivalent parameters calculated by the coupled single-port method. Compared to conventional methods, the proposed method requires fewer PMU measurements and provides more accurate margin estimates. Case studies on extensive test systems validate the accuracy of the proposed method. The comparison between the conventional coupled single-port method and the developed method is also provided to demonstrate the effectiveness of the new method.

Q2

1 Introduction

The ability to maintain voltage stability is an important property of a secure and resilient power system. With the increasing load consumption and penetration of renewable energy resources, power systems are being operated with less margin to voltage stability limits [1]. The assessment of voltage stability has become a major concern for the power system planning and operation. Voltage stability can be classified into two categories: dynamic stability and static stability. The dynamic instability of voltage is analysed by time-domain simulations. The static voltage instability, which is generally triggered by transmission and/or generation outages or by severe load increases, is assessed by steady-state analysis [2]. This paper focuses on the assessment of static voltage stability.

Many approaches have been proposed in the literature on the assessment of static voltage stability, which can be categorised into model-based methods and measurement-based methods [3, 4]. Representative model-based methods include continuation power flow (CPF) [5, 6] and optimal power flow (OPF) [7, 8]. CPF employs a predictor–corrector scheme to systematically trace the solutions of a set of parameterised equations along the bifurcation manifold by increasing the loading level until a voltage stability limit is encountered. OPF-based methods find the loading margin to voltage instability by adopting optimisation-based methods which maximise the loading factor while satisfying a set of operation constraints such as the power flow equations, bus-voltage limits, thermal limits of transmission lines and reactive power limits of generators. The complexity of system models and the computational burden make these methods difficult to be implemented in real-time or a decentralised manner.

In recent years, the wide deployment of phasor measurement units (PMUs) and the advancement in communication infrastructures have facilitated the development of measurement-based stability assessment. Many measurement-based methods rely on the impedance matching condition, i.e. a Thévenin-like equivalent system model can be derived at load buses, voltage instability occurs if the identified load impedance matches the estimated system Thévenin impedance according to the maximum power transfer principle [9]. The measurement-based methods can be further classified into decentralised and centralised ones. The decentralised methods are based on local measurements from a single PMU with few or no information exchange with its neighbouring PMUs. The study in [10] proposes a local voltage stability assessment method by estimating Thévenin equivalent parameters based on phasor measurements. This work is extended in [11] by measuring the load impedances in the direction of the bulk load instead of the local load. A method to quantify uncertainties of phasor measurements in stability assessment is proposed in [12], and a robust state estimation-based technique is introduced in [13] to mitigate the effect of measurement noise. Tellegen's theorem is applied to calculate Thévenin parameters based on two consecutive phasor measurements of voltage and current in [14]. The authors of [15] propose a real-time algorithm to identify Thévenin parameters by updating the Thévenin voltage per the load impedance variation. Parniani and Vanouni [16] propose a local voltage stability index that relies on scalar local measurements. The centralised assessment methods leverage the wide-area measurements from networked PMUs to monitor voltage stability. The study in [17] integrates the information of reactive power reserves of generators with the local voltage stability assessment to improve the stability margin estimation. Necessary conditions that ensuring the voltage stability in distribution systems have been proposed in [18, 19]. The authors in [2] proposed a method to fit a set of algebraic equations to the sampled states and perform sensitivity analysis to detect the operating point with the maximum load power.

The studies in [9, 20, 21] propose a coupled single-port model which decouples a meshed power system into individual single generator versus single bus network and directly calculates Thévenin parameters using phasor measurements at all load and generator buses. The method has been modified in [22, 23] by considering disproportionally-increasing loads and generation equivalent models. The coupled single-port model is also referred to as multi-port Thévenin equivalent since it maintains the characteristics of individual generators and loads instead of lumping them into a single equivalent [3, 11].

In this paper, it is identified that the prevailing impedance matching condition fails to detect the onset of voltage instability in certain cases. In particular, the impedance matching condition is not applicable to cases where equivalent parameters are obtained

© The Institution of Engineering and Technology 2017

from static system equivalencing techniques. A major issue with the coupled single-port method is that voltage instability may happen before or after the impedance matching point in certain cases, which leads to inaccurate estimation of the voltage stability margin. In this paper, this phenomenon is named as impedance crossing. To reveal the nature of the impedance crossing issue, we provide a detailed sensitivity analysis of load consumption with respect to system loading factors. It is shown that the impedance matching condition holds when system equivalent parameters are constant. However, the condition may not hold when both the equivalent voltage and equivalent impedance are functions of the system parameters. An improved coupled single-port method is proposed in this paper to improve the accuracy of the coupled single-port method. Adjustments to the equivalent parameters of a load bus are calculated from two consecutive phasor measurements at the corresponding bus to capture the power system evolution. The objectives of the proposed method are to improve the accuracy of margin estimates and to ensure that the impedance matching condition is met at the loadability point. The proposed method only requires communications with PMUs at generator buses, which reduces the complexity of communication infrastructures. Since the proposed method does not require the implicit assumption of proportional load increase as in [9], we expect the margin estimates to be more accurate when load powers change disproportionally.

The remaining of this paper is organised as follows. Section 2 presents the technical background and gives a brief introduction to the coupled single-port method. Section 3 identifies the problems associated with the coupled single-port method and proposes an improved method with theoretical foundations. In Section 4, numerical results demonstrating the problems with the conventional method and the effectiveness of the proposed method are provided. Section 5 concludes the paper with the major findings.

2 Background

2.1 System modelling

The general power system model used in voltage stability analysis can be described as a set of differential-algebraic equations (DAE)

$$\dot{x} = f(x, y, \lambda, p), \tag{1a}$$

$$0 = f(x, y, \lambda, p), \tag{1b}$$

where $\boldsymbol{x} \in \mathbb{R}^m$ is a vector of system states associated with dynamics of system elements, such as generator and load dynamics. $\boldsymbol{y} \in \mathbb{R}^n$ is a vector of steady-state system states, such as load voltage magnitudes and angles, and generator voltage angles. $\boldsymbol{\lambda} \in \mathbb{R}^q$ is a vector of uncontrollable system variables, such as system loading factors. $\boldsymbol{p} \in \mathbb{R}^p$ is a vector of controllable system variables, such as the real and reactive powers of base load, the real power output and voltage magnitudes of generators, and the tap positions of load tap changers. $f: \mathbb{R}^m \times \mathbb{R}^n \times \mathbb{R}^q \times \mathbb{R}^p \to \mathbb{R}^m$, $g: \mathbb{R}^m \times \mathbb{R}^n \times \mathbb{R}^q \times \mathbb{R}^p \to \mathbb{R}^{n+p+q}$ are C^∞ (smooth) functions.

The equilibria of the above DAE model satisfy

$$0 = f(x, y, \lambda, p), \tag{2a}$$

$$0 = f(x, y, \lambda, p)\,. \tag{2b}$$

Assume the Jacobian $D_x f$ is invertible for every solution $(x_0, y_0, \lambda_0, p_0)$ of (2a), we have the following conclusion based on the implicit function theorem: there exists a function h and a radius $r > 0$ such that for solutions $(x, y, \lambda, p) \in \text{Ball}((x_0, y_0, \lambda_0, p_0), r)$, $x = h(y, \lambda, p)$.

Let $g(h(y, \lambda, p), y, \lambda, p) = \tilde{g}(y, \lambda, p)$ and assume $\boldsymbol{y} \in \mathbb{R}^n$ represents voltage magnitudes and angles of loads, as well as voltage angles of all generators except the one at the slack bus. In addition, let $\boldsymbol{\lambda} \in \mathbb{R}^q$ be a parameter vector of real and reactive load powers. Then the system is modelled by

$$0 = \tilde{g}(y, \lambda, p) \tag{3}$$

which is the well-known power flow model of a power system. Proportional load increasing model is assumed throughout the paper such that given a base case operating point (y_0, λ_0, p_0), the loading parameter λ at any operating point is a scalar multiple of λ_0, i.e. there exists $\kappa > 0$ such that $\lambda = \kappa\lambda_0$. In this case $q = 1$ and $\lambda \in \mathbb{R}$.

Dobson [24] shows that in general (1) has a saddle-node bifurcation at $(x^*, y^*, \lambda^*, p^*)$ if and only if (3) has a saddle-node bifurcation at (y^*, λ^*, p^*). Since voltage stability is primarily related to the saddle-node bifurcation of dynamical systems, without loss of generality, (3) is used in this paper for voltage stability analysis.

A power system represented by (3) undergoes a saddle-node bifurcation at $\lambda = \lambda^*$ when

$$0 = \tilde{g}(z^*), \tag{4a}$$

$$0 = D_y\tilde{g}(z^*)^{\mathrm{T}}\boldsymbol{v} = D_y\tilde{g}(z^*)\boldsymbol{w}, \tag{4b}$$

$$0 \neq D_\lambda\tilde{g}(z^*)\boldsymbol{w}, \tag{4c}$$

$$0 \neq w^{\mathrm{T}}[D_y(D_y\tilde{g}(z^*))\boldsymbol{v}]\boldsymbol{v}, \tag{4d}$$

where $\boldsymbol{v}$ and $\boldsymbol{w}$ are normalised right and left eigenvectors of the Jacobian $D_y\tilde{g}(z^*)$, and $z^* = (y^*, \lambda^*, p^*)$ is the bifurcation point. Equations (4c) and (4d) are the transversality and non-degeneracy conditions, respectively [25]. The set of all such λ^* amounts to the q-dimensional loadability surface $\boldsymbol{\Sigma}$.

At an operating point (y, λ, p), the system loading margin is defined as the real number $k > 0$ such that $\lambda^* = (1 + k)\lambda_0 \in \Sigma$.

2.2 Sensitivity analysis

Sensitivity analysis is used to analyse the variation of equivalent parameters with respect to the system loading condition [26]. Let η be an element in the set of equivalent parameters, e.g. $\eta \in (|Z_{\text{eq}}|, |E_{\text{eq}}|, \angle Z_{\text{eq}})$ where $\boldsymbol{E}_{\text{eq}}$ and $\boldsymbol{Z}_{\text{eq}}$ are the vectors of equivalent voltages and equivalent impedances seen from all load buses, respectively. Assume that p is constant, we have $\eta = \eta(y, \lambda)$.

The incremental change of $\eta(y, \lambda)$ with respect to y and λ is

$$\mathrm{d}\eta = (\mathrm{d}y)^{\mathrm{T}}\frac{\partial\eta}{\partial y} + \frac{\partial\eta}{\partial\lambda}\mathrm{d}\lambda = \mathrm{d}\lambda\left(\frac{\partial\eta}{\partial\lambda} - (D_\lambda^{\mathrm{T}}\tilde{g})(D_y^{\mathrm{T}}\tilde{g})^{-1}\frac{\partial\eta}{\partial y}\right). \tag{5}$$

The inverse of the Jacobian $D_y\tilde{g}$ is

$$(D_y\tilde{g})^{-1} = \boldsymbol{V}\boldsymbol{\Sigma}^{-1}\boldsymbol{W} = \sum_{i=1}^{n}\frac{v_i w_i^{\mathrm{T}}}{\sigma_i}, \tag{6}$$

where $\boldsymbol{V}$ and $\boldsymbol{W}$ are the matrices of right and left eigenvectors of $D_y\tilde{g}$, respectively, $\boldsymbol{\Sigma}$ is a diagonal matrix containing eigenvalues of $D_y\tilde{g}$, and $\boldsymbol{v}_i$ and $\boldsymbol{w}_i$ are the ith right and left eigenvectors of $D_y\tilde{g}$, respectively.

Substituting the transpose of (6) into (5) yields

$$\mathrm{d}\eta = \mathrm{d}\lambda\left[\frac{\partial\eta}{\partial\lambda} - (D_\lambda^{\mathrm{T}}\tilde{g})\left(\sum_{i=1}^{n}\frac{w_i v_i^{\mathrm{T}}}{\sigma_i}\right)\frac{\partial\eta}{\partial y}\right]. \tag{7}$$

Therefore, the sensitivity of η with respect to λ is

$$\frac{\mathrm{d}\eta}{\mathrm{d}\lambda} = \frac{\partial\eta}{\partial\lambda} - (D_\lambda^{\mathrm{T}}\tilde{g})\left(\sum_{i=1}^{n}\frac{w_i v_i^{\mathrm{T}}}{\sigma_i}\right)\frac{\partial\eta}{\partial y}. \tag{8}$$

Since the Jacobian $D_y\tilde{g}$ is singular at the bifurcation point according to (4b) and $1/\sigma_{\min} \to +\infty$ as $\det D_y\tilde{g} \to 0$, we have $\mathrm{d}\eta/\mathrm{d}\lambda \to +\infty$ as $\det D_y\tilde{g} \to 0$.

© The Institution of Engineering and Technology 2017

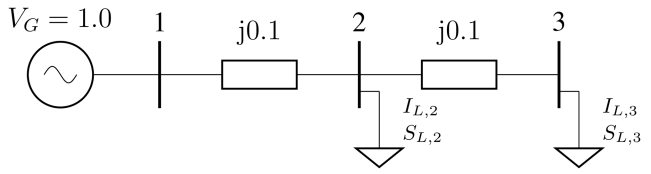

Fig. 1 *Three-bus system*

2.3 Coupled single-port method

Equation (3) can be explicitly described by the following coupled single-port form as:

$$\begin{bmatrix} -I_{\mathrm{L}} \\ I_{\mathrm{G}} \end{bmatrix} = \boldsymbol{Y}\begin{bmatrix} \boldsymbol{V}_{\mathrm{L}} \\ V_{\mathrm{G}} \end{bmatrix} = \begin{bmatrix} Y_{\mathrm{LL}} & Y_{\mathrm{LG}} \\ Y_{\mathrm{GL}} & Y_{\mathrm{GG}} \end{bmatrix}\begin{bmatrix} \boldsymbol{V}_{\mathrm{L}} \\ V_{\mathrm{G}} \end{bmatrix} \tag{9}$$

where $\boldsymbol{Y}$ is the system admittance matrix, $\boldsymbol{V}$ and $\boldsymbol{I}$ are bus voltage and current vectors, respectively, and the subscript L and G represent load and generator buses, respectively.

Let $\mathcal{N} = \{1, 2, \ldots, N\}$ be the set of load buses and $\mathcal{G} = \{N+1, N+2, \ldots, N+M\}$ be the set of generator buses. Then $V_{\mathrm{L}} \in \mathbb{C}^N$ and $V_{\mathrm{G}} \in \mathbb{C}^M$.

The load voltage vector$\boldsymbol{V}_{\mathrm{L}}$ can be expressed as a function of V_{G} and I_{L} as shown below:

$$\boldsymbol{V}_{\mathrm{L}} = \boldsymbol{K}V_{\mathrm{G}} - \boldsymbol{Z}_{\mathrm{LL}}I_{\mathrm{L}}, \tag{10}$$

where $\boldsymbol{K} = -Y_{\mathrm{LL}}^{-1}Y_{\mathrm{LG}} \in \mathbb{C}^{N\times M}$ and $\boldsymbol{Z}_{\mathrm{LL}} = Y_{\mathrm{LL}}^{-1} \in \mathbb{C}^{N\times N}$.

For a load bus $j \in \mathcal{N}$, the bus voltage can be calculated as

$$\begin{aligned} V_{\mathrm{L},j} &= [\boldsymbol{K}V_{\mathrm{G}}]_j - \sum_{i=1}^{k} Z_{\mathrm{LL},jj}I_{\mathrm{L},i} \\ &= [\boldsymbol{K}V_{\mathrm{G}}]_j - \left(Z_{\mathrm{LL},jj} + \sum_{i=1, i\neq j}^{N} Z_{\mathrm{LL},ji}\frac{I_{\mathrm{L},i}}{I_{\mathrm{L},j}}\right)I_{\mathrm{L},j}, \end{aligned} \tag{11}$$

where $[\boldsymbol{K}V_{\mathrm{G}}]_j$ and $Z_{\mathrm{LL},jj} + \sum_{i=1, i\neq j}^{N} Z_{\mathrm{LL},ji}I_{\mathrm{L},i}/I_{\mathrm{L},j}$ are the system equivalent voltage and impedance seen from bus j, respectively.

$\boldsymbol{K}$ and $\boldsymbol{Z}_{LL}$ are matrices derived from the system admittance matrix, and are constant as long as the system topology remains the same. The magnitude of generator voltage $|V_{\mathrm{G}}|$ is constant if the PV–PQ transition of generators is not taken into account. Thus, the magnitude of the system equivalent voltage seen from a load bus j, i.e. $E_{\mathrm{eq},j} = [\boldsymbol{K}V_{\mathrm{G}}]_j$, is relatively constant. In addition, the system equivalent impedance $Z_{\mathrm{eq},j} = Z_{\mathrm{LL},jj} + \sum_{i=1, i\neq j}^{N} Z_{\mathrm{LL},ji}I_{\mathrm{L},i}/I_{\mathrm{L},j}$ is relatively constant when proportional load increasing model is used [9].

The load consumption cannot be further increased beyond the loadability limit point because of the system constraints, and the point corresponds to the saddle-node bifurcation point of the system [26]. A load bus reaches its loadability limit when the load impedance and the system equivalent impedance seen from the local load are equal in magnitude ($|Z_{\mathrm{L}}| = |Z_{\mathrm{eq}}|$), which is known as the impedance matching condition [9].

3 Improved coupled single-port method

3.1 Issue with impedance matching condition

The impedance matching condition is satisfied at the loadability limit for a radial two-bus system, as demonstrated in [26, 27], where the equivalent voltage and the equivalent impedance are constant. However, the equivalent voltage and impedance derived from the coupled single-port model for a multi-bus system are system-dependent, i.e. the equivalent voltage and impedance vary with the system loading condition. There is no guarantee that the loadability limit coincides with the impedance matching condition when system equivalent parameters are not constant.

3.1.1 Example: To demonstrate the above mentioned argument, numerical results based on an example system are provided. Consider a radial three-bus system with one generator and two constant power loads in Fig. 1. Suppose $V_1 = 1$, $Z_{\mathrm{line1}} = Z_{\mathrm{line2}} = \mathrm{j}0.1$, $V_2 = 0.7 - \mathrm{j}0.3$, and $V_3 = 0.5 - \mathrm{j}0.5$. Given the operating condition, load powers, currents and impedances are $S_{\mathrm{L},2} = 1 + \mathrm{j}0.4$, $S_{\mathrm{L},3} = 2$, $I_{\mathrm{L},2} = 1 - \mathrm{j}$, $I_{\mathrm{L},3} = 2 - \mathrm{j}2$, $Z_{\mathrm{L},2} = 0.5 + \mathrm{j}0.2$, $Z_{\mathrm{L},3} = 0.25$.

The equivalent impedances seen from buses 2 and 3 are calculated as

$$Z_{\mathrm{eq},2} = Z_{\mathrm{LL},11} + Z_{\mathrm{LL},12}\frac{I_3}{I_2} = \mathrm{j}0.3 \tag{12a}$$

$$Z_{\mathrm{eq},3} = Z_{\mathrm{LL},22} + Z_{\mathrm{LL},21}\frac{I_2}{I_3} = \mathrm{j}0.25 \tag{12b}$$

The magnitudes of the load impedance and the equivalent impedance at bus 3 are equal. Based on the coupled single-port method, the loadability limit point is encountered under the current operating condition. However, the determinant of the power flow Jacobian is

$$\det J = \begin{vmatrix} 12 & -5 & -1.3131 & 2.8284 \\ -5 & 5 & -2.6261 & -2.8284 \\ -1 & -2 & 14.7063 & -7.0711 \\ 2 & -2 & 6.5653 & 7.0711 \end{vmatrix} = 301.57 \neq 0. \tag{13}$$

Since the determinant is non-zero, the system has yet reached its loadability limit under the given operating condition, even though the impedance matching condition is met.

Recently, we have shown in [18] that the singularity of the power flow Jacobian for the above system coincides with the singularity of the complex Jacobian matrix defined as (see (14))

Plugging in the values given above, we have

$$\boldsymbol{J}_c = \begin{bmatrix} V_2 & 0 & -Z_{\mathrm{line1}}I_{\mathrm{L},2} & -Z_{\mathrm{line1}}I_{\mathrm{L},3} \\ 0 & V_3 & -Z_{\mathrm{line1}}I_{\mathrm{L},2} & -(Z_{\mathrm{line1}} + Z_{\mathrm{line2}})I_{\mathrm{L},3} \\ -Z_{\mathrm{line1}}^*I_{\mathrm{L},2}^* & -Z_{\mathrm{line1}}^*I_{\mathrm{L},3}^* & V_2^* & 0 \\ -Z_{\mathrm{line1}}^*I_{\mathrm{L},2}^* & -(Z_{\mathrm{line1}} + Z_{\mathrm{line2}})^*I_{\mathrm{L},3}^* & 0 & V_3^* \end{bmatrix}. \tag{14}$$

© The Institution of Engineering and Technology 2017

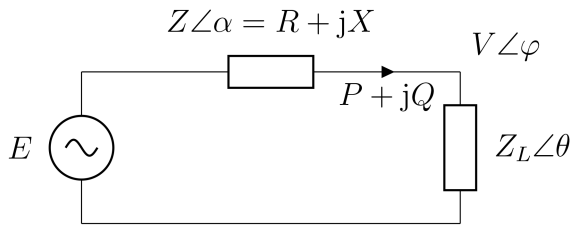

Fig. 2 *Two-bus system*

$$\boldsymbol{J}_c = \begin{bmatrix} 0.7 - \mathrm{j}0.3 & 0 & -(0.1 + \mathrm{j}0.1) & -(0.2 + \mathrm{j}0.2 \\ 0 & 0.5 - \mathrm{j}0.5 & -(0.1 + \mathrm{j}0.1) & -(0.4 + \mathrm{j}0.4 \\ -(0.1 - \mathrm{j}0.1) & -(0.2 - \mathrm{j}0.2) & 0.7 + \mathrm{j}0.3 & 0 \\ -(0.1 - \mathrm{j}0.1) & -(0.4 - \mathrm{j}0.4) & 0 & 0.5 + \mathrm{j}0.5 \end{bmatrix} \quad (15)$$

.

It is easy to see that the Jacobian matrix (15) is diagonally dominance but not strictly diagonally dominance, since $|J_{c,22}| = |J_{c,23}| + |J_{c,24}|$. We notice that the sum of off-diagonal elements is in fact the voltage drop across the equivalent impedance. Realising the impedance matching condition is satisfied when the voltage drop and load voltage have the same magnitude, we see that when all off-diagonal elements are in phase, the impedance matching condition is simply the condition of weak diagonal dominance of the Jacobian matrix $\boldsymbol{J}_c$. For example, in a DC system, the off-diagonal element are always in phase, thus the impedance matching condition becomes a necessary condition for system instability. For an AC system the situation is different from the off-diagonal elements are not necessarily in phase, and the presence of PV buses further complicates the problem, as discussed in [18].

3.1.2 Theoretical analysis: For a two-bus system as shown in Fig. 2, the load voltage V can be described as a function of load power P and Q:

$$|V|^4 - [|E|^2 - 2(RP + XQ)]|V|^2 + (P^2 + Q^2)(R^2 + X^2) = 0. \quad (16)$$

According to [26], the loadability point of the two-bus system coincides with the maximum power transfer point, and is achieved when (16) has repeated roots

$$[|E|^2 - 2(RP + XQ)]^2 - 4(P^2 + Q^2)(R^2 + X^2) = 0. \quad (17)$$

By solving (16) for V at the loadability point, we have

$$|V|^2 = \sqrt{(P^2 + Q^2)(R^2 + X^2)} = |S||Z|, \quad (18)$$

where $|Z| = \sqrt{R^2 + X^2}$ and $|S| = \sqrt{P^2 + Q^2}$.

On the other hand, let the magnitude of the load impedance be $|Z_\mathrm{L}|$, the load voltage can be represented as

$$|V|^2 = |S||Z_\mathrm{L}|. \quad (19)$$

By comparing (18) and (19), it is concluded that for the two-bus system, the load impedance and the line impedance are equal in magnitude at the loadability point

$$|Z| = |Z_\mathrm{L}|. \quad (20)$$

We will show in the sequel that, in general, the above maximum power transfer condition (17) and the impedance matching condition (20) cannot be generalised to multi-bus systems with varying equivalent voltages and impedances.

The real power delivered to a load bus i at any time can be expressed by the equivalent voltage $E_{\mathrm{eq},i}$ and the impedance $Z_{\mathrm{eq},i}$ seen from the load bus as

$$\begin{aligned} P_i &= |I_i||Z_i|\cos\theta_i \\ &= \frac{|E_{\mathrm{eq},i}|^2\cos\theta_i}{|Z_{\mathrm{eq},i}|^2/|Z_i| + |Z_i| + 2|Z_{\mathrm{eq},i}|\cos(\alpha_i - \theta_i)}, \end{aligned} \quad (21)$$

where α_i is the angle of equivalent impedance, and $\cos\theta_i$ is the load power factor.

The real power consumption at bus $j \in \mathcal{N}$ is a scalar multiple of λ. Let the multiplier be ℓ, then $P_j = \ell\lambda$. Hence

$$\begin{aligned} \frac{\mathrm{d}P_j(|E_{\mathrm{eq},j}|, |Z_{\mathrm{eq},j}|, |Z_j|, \alpha_j)}{\mathrm{d}\lambda} &= \frac{\partial P_j}{\partial|E_{\mathrm{eq},j}|}\frac{\mathrm{d}|E_{\mathrm{eq},j}|}{\mathrm{d}\lambda} + \frac{\partial P_j}{\partial|Z_{\mathrm{eq},j}|}\frac{\mathrm{d}|Z_{\mathrm{eq},j}|}{\mathrm{d}\lambda} \\ &\quad + \frac{\partial P_j}{\partial|Z_j|}\frac{\mathrm{d}|Z_j|}{\mathrm{d}\lambda} + \frac{\partial P_j}{\partial\alpha_j}\frac{\mathrm{d}\alpha_j}{\mathrm{d}\lambda} \\ &= \ell. \end{aligned} \quad (22)$$

From (21)

$$\frac{\partial P_j}{\partial|E_{\mathrm{eq},j}|} = \frac{2|E_{\mathrm{eq},j}|\cos\theta_j}{|Z_{\mathrm{eq},j}|^2/|Z_j| + |Z_j| + 2|Z_{\mathrm{eq},j}|\cos(\alpha_j - \theta_j)} > 0, \quad (23a)$$

$$\frac{\partial P_j}{\partial|Z_{\mathrm{eq},j}|} = -\gamma\left(\frac{2|Z_{\mathrm{eq},j}|}{|Z_j|} + 2\cos(\alpha_j - \theta_j)\right) < 0, \quad (23b)$$

$$\frac{\partial P_j}{\partial|Z_j|} = \gamma\left(\frac{|Z_{\mathrm{eq},j}|^2}{|Z_j|^2} - 1\right) < 0, \quad (23c)$$

$$\frac{\partial P_j}{\partial\alpha_j} = 2\gamma|Z_{\mathrm{eq},j}|\sin(\alpha_j - \theta_j), \quad (23d)$$

where

$$\gamma = \frac{|E_{\mathrm{eq},j}|^2\cos\theta_j}{\left(|Z_{\mathrm{eq},j}|^2/|Z_j| + |Z_j| + 2|Z_{\mathrm{eq},j}|\cos(\alpha_j - \theta_j)\right)^2} > 0. \quad (24)$$

The signs of (23) are determined based on the assumptions that $0 < \theta_j < \alpha_j < \pi/2$ and $|Z_{\mathrm{eq},j}| < |Z_j|$.

If $E_{\mathrm{eq},j}$ and $Z_{\mathrm{eq},j}$ are constant, then (22) reduces to

$$\frac{\mathrm{d}P_j(|Z_j|)}{\mathrm{d}\lambda} = \frac{\mathrm{d}P_j}{\mathrm{d}|Z_j|}\frac{\mathrm{d}|Z_j|}{\mathrm{d}\lambda} = \ell, \quad (25)$$

at the loadability point. We know from the sensitivity analysis that $\mathrm{d}|Z_j|/\mathrm{d}\lambda \to -\infty$ as the system approaches the loadability point. Therefore, $\mathrm{d}P_j/\mathrm{d}|Z_j| \to 0$ as the loadability limit is approached, which implies $|Z_{\mathrm{eq},j}| = |Z_j|$ based on (23c).

However, when $E_{\mathrm{eq},j}$ and $Z_{\mathrm{eq},j}$ are functions of λ, $\partial P_j/\partial|Z_j|$ may not approach zero as the system approaches the loadability limit.

For example, we may assume that $\mathrm{d}|E_{\mathrm{eq},j}|/\mathrm{d}\lambda < 0$ and that $Z_{\mathrm{eq},j}$ is a constant. Based on (22), we have

© The Institution of Engineering and Technology 2017

$$\frac{\partial P_j}{\partial |E_{\text{eq},j}|}\frac{\mathrm{d}|E_{\text{eq},j}|}{\mathrm{d}\lambda}+\frac{\partial P_j}{\partial |Z_j|}\frac{\mathrm{d}|Z_j|}{\mathrm{d}\lambda}=\ell. \tag{26}$$

It is known from the sensitivity analysis that $\mathrm{d}|E_{\text{eq},j}|/\mathrm{d}\lambda \to -\infty$ and $\mathrm{d}|Z_j|/\mathrm{d}\lambda \to -\infty$ as the system approaches the loadability limit. In addition, we know from (23a) that $\partial P_j/\partial |E_{\text{eq},j}| > 0$ always holds. By inspection, we know that

$$\frac{\partial P_j}{\partial |Z_j|}=\left(\frac{\mathrm{d}|Z_j|}{\mathrm{d}\lambda}\right)^{-1}\left(\ell-\frac{\partial P_j}{\partial |E_{\text{eq},j}|}\frac{\mathrm{d}|E_{\text{eq},j}|}{\mathrm{d}\lambda}\right)<0 \tag{27}$$

holds as the loadability limit is approached, which implies

$$\frac{|Z_{\text{eq},j}|}{|Z_j|}=\sqrt{1+\frac{\partial P_j/\partial |Z_j|}{\gamma}}<1. \tag{28}$$

Equation (28) indicates that the magnitude of the load impedance $|Z_j|$ is larger than the magnitude of the equivalent impedance $|Z_{\text{eq},j}|$ at the loadability point.

Similarly, by assuming that $\mathrm{d}\alpha_j/\mathrm{d}\lambda \to \infty$ as the system approaches the loadability point, and $|E_{\text{eq},j}|$ and $|Z_{\text{eq},j}|$ are constant, we may find that $|Z_j| < |Z_{\text{eq},j}|$ at the loadability point.

In general, when both $\boldsymbol{E}_{\text{eq}}$ and $\boldsymbol{Z}_{\text{eq}}$ are functions of λ, the impedance matching condition (20) does not necessarily hold at the loadability point. The load impedance and the equivalent impedance can match either before or after the loadability limit, which depends on the sensitivities of magnitude of equivalent voltage and angle of equivalent impedance. Therefore, the conventional coupled single-port-based voltage stability indicator may overestimate or underestimate voltage stability margins.

3.2 Proposed method and solution algorithm

The conventional coupled single-port method is a steady-state system equivalencing technique. However, we have shown in Section 3.1 that this method cannot model system responses to load variations. To obtain a better voltage stability margin estimate, it is necessary to find an equivalent voltage $E'_{\text{eq},j}$ and an equivalent impedance $Z'_{\text{eq},j}$ seen from the load bus j that not only satisfy the static network flow given by (16), but also reflect the system's responses to load variations.

Let the voltage phasors measured at bus j at two consecutive time stamps t_0 and t_1 be $V_j(t_0)$ and $V_j(t_1)$, the real power consumption at load bus j at the two time stamps be $P_j(t_0)$ and $P_j(t_1)$. If $t_1 - t_0$ is small, the voltage sensitivity with respect to the loading factor λ is approximated by

$$\frac{\mathrm{d}|V_j|}{\mathrm{d}\lambda}=\frac{|V_j(t_0)|-|V_j(t_1)|}{P_j(t_0)-P_j(t_1)}. \tag{29}$$

Specifically

$$\left(\frac{\partial P_j(E'_{\text{eq},j},Z'_{\text{eq},j},V_j)}{\partial |V_j|}\right)^{-1}=\frac{\mathrm{d}|V_j|}{\mathrm{d}\lambda} \tag{30}$$

In (29) and (30), the use of real power in capturing the system response to load variation is equivalent to using reactive power when the ratio of load real and reactive power variations is known. As commonly seen in the voltage stability analysis, we assume that the load real and reactive powers increases proportionally in the study, so the variation of real and reactive powers has the same implication in terms of load changes. This assumption is well-justified for large-scale power systems where the single loads are actually aggregations of smaller loads. Therefore the power factors are almost constant statistically. In fact, an almost identical algorithm can be derived with the use of reactive power variation.

While PMUs sample at tens of samples per second, long-term voltage instability occurs over tens of seconds to tens of minutes. So there is a large separation of time-scales between PMU sampling and the evolution of voltage instability. We have assumed throughout the paper that high-quality measurements are available and we do not distinguish between measured and true values. However, in practical systems, it has been shown that frequent sampling may bring adverse effects to system equivalent parameter estimation due to insufficient system dynamic evolution and high proportion of measurement noise [28]. When PMU measurement quality is determined to be an issue, a state estimation and filtering layer [29] can be implemented between the raw measurements and our algorithm to improve signal-to-noise ratios and reject bad data. In the context of voltage stability monitoring through system equivalents, least square and recursive least square estimation have been proposed to deal with measurement noise and system transients [2, 17]. The determination of sampling rate should be conducted on a case-by-case basis, but we argue that it should not be less than once per few seconds to allow for appreciable system load variation.

In addition to (30), $E'_{\text{eq},j}$ and $Z'_{\text{eq},j}$ should also satisfy the power flow (16) for the equivalent two-bus system

$$\begin{aligned}&|V_j|^4-[|E'_{\text{eq},j}|^2-2(R_{\text{eq},j}P_j+X_{\text{eq},j}Q_j)]|V_j|^2+(P_j^2+Q_j^2)\\&(R_{\text{eq},j}^2+X_{\text{eq},j}^2)=0,\end{aligned} \tag{31}$$

where $Z'_{\text{eq},j}=R_{\text{eq},j}+\mathrm{j}X_{\text{eq},j}$, and the load power consumption is $S_j=P_j+\mathrm{j}Q_j$.

The equivalent voltage and impedance that satisfy (30) and (31) provide accurate system responses to local load variations. Equation (31) describes the power flow equation of the equivalent two-bus system. However, there are infinite number of equivalent parameter pairs $(\boldsymbol{E}_{\text{eq}},\boldsymbol{Z}_{\text{eq}})$ that satisfy the power flow equations, including the one given by the conventional coupled single-port method. Among them, we would like to find one that also describes the voltage variation with respect to load variation. That is, we want to find the pair of equivalent parameters that satisfies (30), which describes the fact that the equivalent parameters should behave such that when taking partial derivatives of the real power with respect to voltage, the response given by the equivalent parameters should match that given by the measurement. The parameters estimated in this way have certain advantages over the conventional ones. First, as will be shown in the sequel, the improved model guarantees that the loadability point detection is exact. Second, the incorporation of the load response information facilitates the estimation of equivalent parameters from a limited number of PMUs with comparable (or even better) margin estimation accuracy. The comparison of stability margin is deferred to Section 4.

Let the left hand side of (31) be F, then the total derivative of F is

$$\mathrm{d}F=\frac{\partial F}{\partial P_j}\mathrm{d}P_j+\frac{\partial F}{\partial |V_j|}\mathrm{d}|V_j|=0. \tag{32}$$

Then

$$\gamma=\frac{\mathrm{d}P_j}{\mathrm{d}|V_j|}=-\frac{\partial F/\partial |V_j|}{\partial F/\partial P_j}, \tag{33}$$

where

$$\frac{\partial F}{\partial |V_j|}=4|V_j|^3-2(|E'_{\text{eq},j}|^2-2(R_{\text{eq},j}P_j+X_{\text{eq},j}Q_j))|V_j|, \tag{34a}$$

$$\frac{\partial F}{\partial P_j}=2|V_j|^2(R_{\text{eq},j}+qX_{\text{eq},j})+|Z'_{\text{eq},j}|(2P_j+2q^2P_j), \tag{34b}$$

where $q=Q_j/P_j$.

Substitute (29) and (34) into (33), we have

© The Institution of Engineering and Technology 2017

$$|E'_{\text{eq},j}| = \frac{2-\gamma|V_j|/P_j}{1-\gamma|V_j|/P_j}|V_j|\cos(\theta_e-\theta), \tag{35}$$

where θ and θ_e are the phase angles of the load voltage V_j and the equivalent voltage $E_{\text{eq},j}$, respectively. The detailed derivation of (35) is provided in the Appendix.

Since $\gamma \le 0$ and $|\theta_e - \theta| \le \pi/2$, the magnitude of the equivalent voltage $|E'_{\text{eq},j}|$ given by (35) is well defined.

The equivalent impedance can be derived from the equivalent voltage as

$$Z'_{\text{eq},j} = \frac{E'_{\text{eq},j} - V_j}{I_j}, \tag{36}$$

where $I_j = S_j^*/V_j^*$ is the load current. We note that there is a connection between the proposed method of calculating system equivalent parameters and that in [22], which is the use of sensitivity information in equivalent parameter estimation. However, we also note that in order to obtain the system equivalent parameter estimation seen from a load bus, in addition to local measurements, our method requires only the voltage phasor measurements at generator buses, as opposed to all other load buses in [22]. This simplification amounts to the reduction of PMU communication complexity by an order of magnitude in most cases. The distinction of the proposed method and that in [22] can be realised by observing that in order to calculate the equivalent parameters, the algorithm requires the availability of either $\angle Z_{\text{eq}}$ or $\angle E_{\text{eq}}$. The calculation of $\angle E_{\text{eq}}$ turns out to be easier since much fewer PMU measurements are needed and it is relatively easy to estimate the generator voltage phasors when some of the measurements are unavailable. In addition, system-wide voltage stability can be monitored through only a few weak buses [9, 21, 30], which makes the proposed method even more appealing as PMU measurements at load buses other than the identified weak buses are no longer needed. The estimated system equivalents obtained by the proposed method and that in [22] coincide when the equivalent voltage and impedance are constant.

To ensure the margin is meaningful (i.e. the margin is positive before the loadability point, and is zero at the loadability point), we need $|Z'_{\text{eq},j}| \le |Z_{\text{L},j}|$ where the equality is attained if and only if the margin is zero. To prove that this is true for the proposed method, we show that (35) guarantees the above-mentioned relationship between the two impedances.

Note that $\gamma \le 0$ and the equality is attained if and only if the system is at loadability point, so (35) reduces to

$$|E'_{\text{eq},j}| = 2|V_j|\cos(\theta_e-\theta) \tag{37}$$

at the loadability point.

Let $E'_{\text{eq},j} = E_r + \text{j}E_i$, and $V_j = V_r + \text{j}V_i$, then the line voltage drop is $V_{\text{line},r} = E_r - V_r$ and $V_{\text{line},i} = E_i - V_i$. The sum of squares of the line voltage is

$$\begin{aligned}|V_{\text{line}}|^2 &= V_{\text{line},r}^2 + V_{\text{line},i}^2 \\ &= E_r^2 + E_i^2 + V_r^2 + V_i^2 - 2|E'_{\text{eq},j}||V_j|\cos(\theta_e-\theta) \\ &= |E'_{\text{eq},j}|^2 + |V_j|^2 - 2|E'_{\text{eq},j}||V_j|\cos(\theta_e-\theta).\end{aligned} \tag{38}$$

At the loadability point, (38) reduces to $|V_{\text{line}}| = |V_j|$ based on (37) whereas $|V_{\text{line}}| < |V_j|$ when $\gamma < 0$ and $|E_{\text{eq},j}| < 2|V_j|\cos(\theta_e - \theta)$.

Therefore, we have $|Z'_{\text{eq},j}| = |Z'_{\text{L},j}|$ at the loadability point and $|Z'_{\text{eq},j}| < |Z_{\text{L},j}|$ before the loadability point.

The loading margin to voltage stability at load bus j can be calculated as

$$\text{Margin}_j = P_{j\max} - |I_{\text{L},j}|^2|Z_{\text{L},j}|\cos\theta_j, \tag{39}$$

where the maximum deliverable real power $P_{j\max}$ is given by

$$P_{j\max} = \frac{|E'_{\text{eq},j}|^2}{|Z'_{\text{eq},j} + bZ_{\text{L},j}|^2}|Z'_{\text{eq},j}|\cos\theta_j \tag{40}$$

based on the impedance matching condition.

The system loading margin is the minimum loading margin among all load buses

$$\text{Margin}_{\text{sys}} = \min\{\text{Margin}_j | j \in \mathcal{N}\}, \tag{41}$$

and the weakest bus i is defined as

$$i = \arg\min\{\text{Margin}_j | j \in \mathcal{N}\} \tag{42}$$

The solution algorithm of the proposed method is summarised in Algorithm 1.

Algorithm 1: Algorithm of loading margin calculation at load bus j

1: Develop the conventional multi-port equivalent voltage matrix $\boldsymbol{K}$ in (15) from the system admittance matrix $\boldsymbol{Y}$.
2: Calculate the angle of the equivalent voltage seen from load bus j by $\theta_e = \angle[\boldsymbol{K}\boldsymbol{V}_{\text{G}}]_j$.
3: Calculate the sensitivity γ of load real power P_j with respect to load voltage $|V_j|$ by (29).
4: Calculate the modified equivalent voltage $|E'_{\text{eq},j}|$ with $|V_j|$, P_j, γ, θ_e, and θ from (35).
5: Calculate the equivalent impedance $|Z'_{\text{eq},j}|$ by (36).
6: Calculate the loading margin to voltage stability at bus j from the equivalent model by (39) and (40).
7: Calculate the system loading margin to voltage stability by (41).

4 Simulation results

In this section, two sets of simulations are performed. To demonstrate the loadability limit detection capability of the proposed method and the issue of impedance matching condition, simulations are performed on IEEE 57-bus and 118-bus test systems. In the second part, we compare the accuracy of margin estimation of the proposed method with conventional coupled single-port method, as well as the modified method proposed in [22]. The system models and loading conditions are available in MATPOWER [31].

4.1 Loadability limit detection and issue of impedance matching

In this subsection, all loads increase proportionally with a step size of 1%. Power flow analysis using MATPOWER is performed at each step until power flow fails to converge. The actual loadability point is obtained when power flow diverges. Real power outputs are dispatched among generators proportionally to their real base power.

4.1.1 IEEE 57-bus test system: The IEEE 57-bus test system has 35 loads and 7 generators, three of which are synchronous condensers. The total system base load is $S = 3752 + \text{j}1009$ MVA, the critical loading factor is $\lambda_{\text{cr}} = 1.89$ with the loading pattern and generation dispatch strategy described at the beginning of the section.

Based on the conventional coupled single-port method, bus 31 has the smallest margin estimate and is identified as the weakest bus. Figs. 3 and 4 show the load and equivalent impedances against loading factor for four buses with the smallest margin estimates. It is observed from Fig. 4 that the load and equivalent impedances of bus 31 cross each other before the actual loadability point. Recall the analysis in Section 3.1, assume that the sensitivities of the equivalent voltage and the magnitude of the equivalent impedance against the load consumption are small, the angle of the equivalent

© The Institution of Engineering and Technology 2017

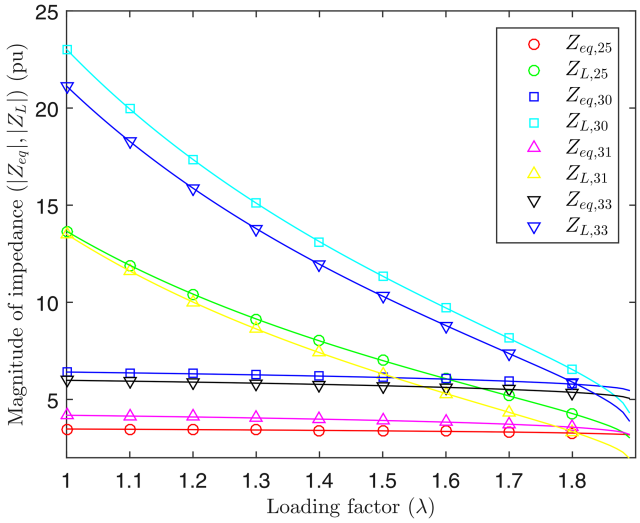

Fig. 3 *Equivalent and load impedances at four load buses with the smallest margin estimates for 57-bus system*

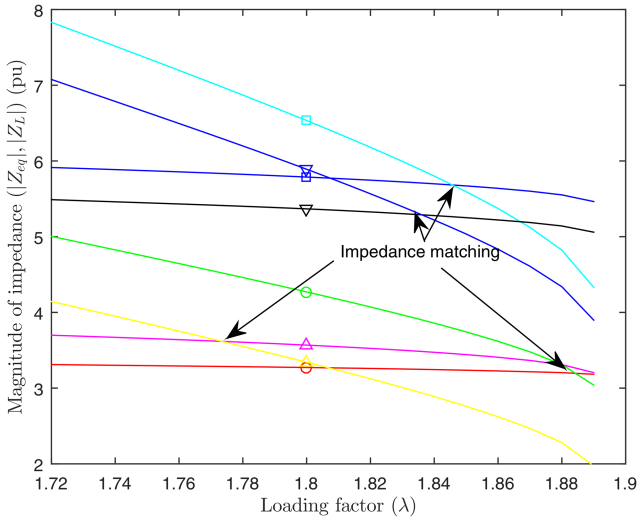

Fig. 4 *Zoom-in of equivalent and load impedances at four load buses with the smallest margin estimates for 57-bus system*

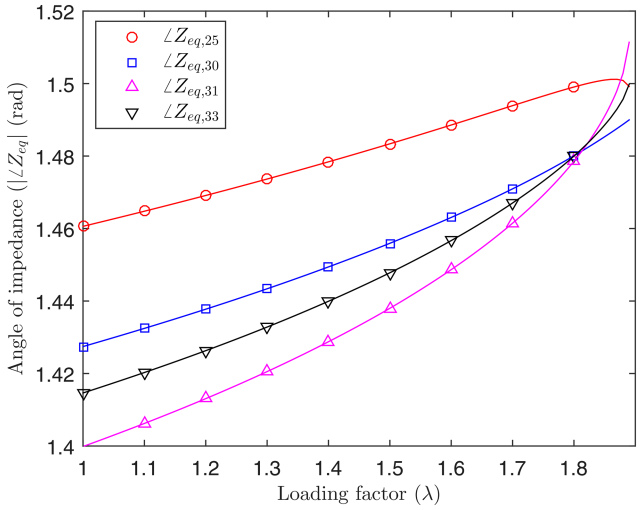

Fig. 5 *Angles of equivalent impedance of four load buses with the smallest margin estimates for 57-bus system*

impedance should be increased when the impedance crossing occurs, which is confirmed in Fig. 5. Note that all load buses with increasing equivalent impedance angles experience the impedance crossing issue. This suggests that the load consumption can be increased as long as the variations of angles of the equivalent impedances are positive. It is further observed that the angle of the equivalent impedance at bus 25 starts to decrease towards the loadability limit, and the system becomes unstable after the impedance crossing happens at bus 25. The margin estimates calculated at the four buses by the conventional coupled single-port method are shown in Fig. 6*a*. Due to the impedance crossing issue, the margin estimates reach zero before the actual loadability point, thus raise false alarm of the voltage instability.

Fig. 6*b* shows the smallest margins estimated by the proposed method. The weakest bus is still identified as bus 31 by the proposed method, which is also in accordance with the result given by modal analysis [20, 32]. Compared to Fig. 6*a*, the estimated margins in Fig. 6*b* approach zero as the system reaches its actual loadability limit.

4.1.2 IEEE 118-bus test system: The IEEE 118-bus test system has 54 loads and 54 generators. The total system base load is $S = 12726 + \text{j}4314\,\text{MVA}$, the critical loading factor is $\lambda_{\text{cr}} = 3.14$.

Based on the conventional coupled single-port method, bus 44 has the smallest margin estimate and is identified as the weakest bus. Fig. 7*a* shows the loading margins estimated by the conventional coupled single-port method. It can be seen that the margin estimates do not reach zero at the loadability point, which is consistent with the analyses in Section 3.1. Since the margin is positive even at the loadability limit, the method fails to detect the onset of voltage instability in this case.

Fig. 7*b* shows the margins estimated by the proposed method. The weakest bus is still identified as bus 44. It is seen from Fig. 7*b* that the estimated margins approach zero as the system approaches the actual loadability point.

4.2 Margin estimation

The primary intention of coupled single-port-based methods is to estimate the loading margin. To this end, we have performed simulations of margin estimation on test cases provided in MATPOWER ranges from 4-bus to 3120-bus systems. Notice that the test cases are only a subset of the available test cases in MATPOWER since we have only chosen test cases where the margins are well defined for the coupled single-port method and the modified method in [22].

4.2.1 Proportional load increase: We first compare accuracy of various methods based on the most commonly used proportional load increase model as in Section 4.1. Table 1 shows the *normalised* loading margins estimated at the initial operating point by coupled single-port method, the modified coupled single-port method in [22], and the proposed method. The actual maximum loading levels are calculated using the Continuation Power Flow solver **`runcpf`** in MATPOWER. The actual (estimated) margin is the difference between the actual (estimated) maximum real power and the current real power, normalised by the current real power. The error is defined as

$$\text{error} = \frac{|\text{estimated margin} - \text{actual margin}|}{\text{actual margin}}.$$

It can be seen that the accuracies of the different methods are comparable and are case dependent. Notice also that the proposed method gives the smallest average error among the three methods. Furthermore, we would like to emphasise again that the proposed method requires only PMU measurements from generator buses, which makes it more attractive for online application with limited PMU availability and communication complexity. In addition, we note that coupled single-port-based methods are heuristic in nature, the original L-index is only exactly when the load currents change proportionally. Thus the margin estimation by coupled single-port model is more accurate when the load current is homogeneous when the system loads are proportionally scaled [18]. This current proportionality condition obviously depends on specific system topology and load characteristics, as will be shown by the next experiment.

© The Institution of Engineering and Technology 2017

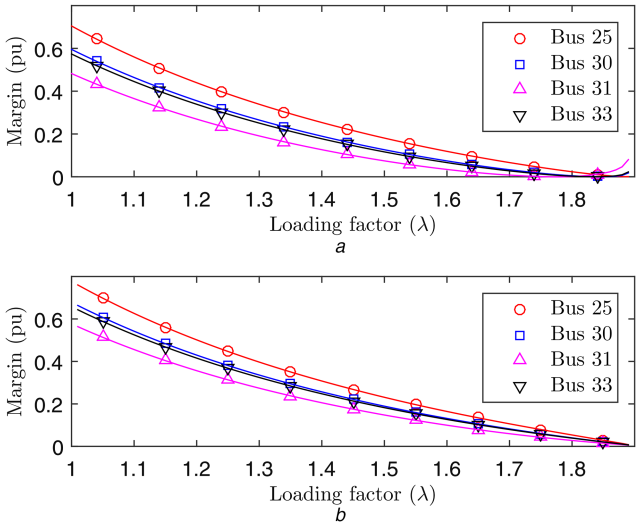

Fig. 6 *Margin estimates at four load buses with the smallest margin estimates for 57-bus system by*
(a) Conventional and ***(b)*** Improved coupled single-port method

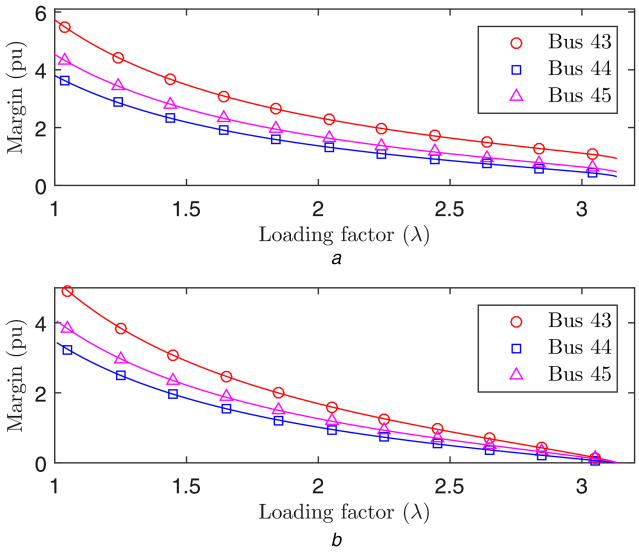

Fig. 7 *Margin estimates at three load buses with the smallest margin estimates for 118-bus system by*
(a) Conventional and ***(b)*** Improved coupled single-port method

Table 1 Comparison of margin estimation on MATPOWER test cases for proportionally-increasing loads

Test case	Estimated margin			Actual margin
	CSP	[22]	Proposed	
case4gs	4.36	4.34	4.35	4.34
case5	13.36	12.35	12.89	9.84
case6ww	2.29	2.32	2.31	2.32
case9	1.45	1.34	1.38	1.49
case14	3.41	3.46	3.44	3.06
case24_ieee_rts	1.43	1.47	1.46	1.28
case30	4.51	4.42	4.43	4.48
case_ieee30	1.69	1.66	1.67	1.96
case39	1.24	1.15	1.20	1.14
case57	0.48	0.58	0.56	0.89
case89pegase	0.88	0.85	0.87	0.86
case118	3.80	3.29	3.42	2.19
case300	0.31	0.32	0.32	0.43
case2383wp	0.57	0.56	0.62	0.89
case3120sp	2.12	0.33	1.92	1.33
average error	0.2206	0.2047	0.1864	—

4.2.2 Disproportional load increase: We have also performed simulations when the loads do not increase proportionally. The constant equivalent impedance assumption in [9] no longer holds in this scenario. However, the proposed method does not rely on this assumption and therefore we expect the proposed method to outperform the one in [9]. To generate the disproportional loading scenario, we set the power increase step of even-numbered buses at 1% of the base load while that of odd-numbered buses is 2%. Under this loading condition, the normalised margins of the odd-numbered buses are twice that of the even-numbered buses. To make the comparison meaningful, we further divide the normalised margins at the odd-numbered buses by two. The simulation results are tabulated in Table 2. It can be seen that the proposed method gives comparable results as the one in [22], while both of these methods are superior to CSP in [9].

5 Conclusion

This paper analyses the problems existing in the conventional coupled single-port method and other Thévenin equivalent-based voltage stability assessment methods. It is mathematically proven that the impedance matching condition underestimates or overestimates loading margins in certain cases. A novel method is proposed to improve the margin estimation of the conventional coupled single-port method by considering voltage-to-load sensitivities in calculating system equivalences. Compared to the conventional methods, it is shown that the new method satisfies the impedance matching condition at loadability limits. Therefore, the loading margin calculated by the improved method can serve as a better indicator of voltage instability. Another salient feature of the proposed method is that PMU measurements are only needed at the generator buses to calculate the system equivalent parameters at a load bus, which reduces the communication complexity. Simulation results show that when system loads experience disproportional variations, the proposed method gives more accurate margin estimates than existing ones.

6 Acknowledgments

This work was supported by the U.S. National Science Foundation (NSF) under the contract ECCS1609080.

© The Institution of Engineering and Technology 2017

Table 2 Comparison of margin estimation on MATPOWER test cases for disproportionally-increasing loads

Test case	Estimated margin			Actual margin
	CSP	[22]	Proposed	
case4gs	2.18	2.17	2.17	2.16
case5	13.36	11.79	12.61	7.61
case6ww	1.14	1.33	1.31	1.36
case9	0.73	0.67	0.69	0.75
case14	2.09	2.37	2.33	1.92
case24_ieee_rts	0.87	0.85	0.86	0.82
case30	2.40	3.24	2.95	3.10
case_ieee30	1.03	1.27	1.26	1.44
case39	0.62	0.74	0.68	0.72
case57	0.24	0.35	0.32	0.53
case89pegase	0.46	0.85	0.67	0.86
case118	2.27	1.92	2.20	1.31
case300	0.18	0.21	0.21	0.25
case2383wp	0.35	0.35	0.49	0.67
case3120sp	1.11	0.28	1.20	0.83
average error	0.3069	0.2170	0.2280	—

7 References

[1] Grijalva, S.: 'Individual branch and path necessary conditions for saddle-node bifurcation voltage collapse', *IEEE Trans. Power Syst.*, 2012, **27**, (1), pp. 12–19

[2] Glavic, M., Van Cutsem, T.: 'Wide-area detection of voltage instability from synchronized phasor measurements. Part I: principle', *IEEE Trans. Power Syst.*, 2009, **24**, (3), pp. 1408–1416

[3] Glavic, M., Van Cutsem, T.: 'A short survey of methods for voltage instability detection'. Proc. IEEE Power and Energy Society General Meeting, San Diego, CA, 24–29 July 2011

[4] Yuan, H., Li, F.: 'A comparative study of measurement-based Thevenin equivalents identification methods'. Proc. North American Power Symp. (NAPS), Pullman, WA, 7–9 September 2014

[5] Ajjarapu, V., Christy, C.: 'The continuation power flow: a tool for steady state voltage stability analysis', *IEEE Trans. Power Syst.*, 1992, **7**, (1), pp. 416–423

[6] Zhou, D.Q., Annakkage, U.D., Rajapakse, A.D.: 'Online monitoring of voltage stability margin using an artificial neural network', *IEEE Trans. Power Syst.*, 2010, **25**, (3), pp. 1566–1574

[7] Avalos, R.J., Cañizares, C.A., Milano, F., *et al.*: 'Equivalency of continuation and optimization methods to determine saddle-node and limit-induced bifurcations in power systems', *IEEE Trans. Circuit Syst. I, Regul. Pap.*, 2009, **56**, (1), pp. 210–223

[8] Karystianos, M.E., Maratos, N.G., Vournas, C.D.: 'Maximizing power system loadability in the presence of multiple binding complementarity constraints', *IEEE Trans. Circuit Syst. I, Regul. Pap.*, 2007, **54**, (8), pp. 1775–1787

[9] Wang, Y., Pordanjani, I.R., Li, W., *et al.*: 'Voltage stability monitoring based on the concept of coupled single-port circuit', *IEEE Trans. Power Syst.*, 2011, **26**, (4), pp. 2154–2163

[10] Vu, K., Begović, M.M., Novosel, D., *et al.*: 'Use of local measurements to estimate voltage-stability margin', *IEEE Trans. Power Syst.*, 1999, **14**, (3), pp. 1029–1035

[11] Cui, B., Begović, M., Nuqui, R., *et al.*: 'On voltage stability monitoring with voltage instability predictor'. Proc. IREP Symp., Rethymnon, Greece, August 2013

[12] Chen, C., Wang, J., Li, Z., *et al.*: 'PMU uncertainty quantification in voltage stability analysis', *IEEE Trans. Power Syst.*, 2015, **30**, (4), pp. 2196–2197

[13] Zhao, J., Wang, Z., Chen, C., *et al.*: 'Robust voltage instability predictor', *IEEE Trans. Power Syst.*, 2017, **11**, (2), pp. 401–408

[14] Smon, I., Verbic, G., Gubina, F.: 'Local voltage-stability index using Tellegen's theorem', *IEEE Trans. Power Syst.*, 2006, **21**, (3), pp. 1267–1275

[15] Corsi, S., Taranto, G.N.: 'A real-time voltage instability identification algorithm based on local phasor Measurements', *IEEE Trans. Power Syst.*, 2008, **23**, (3), pp. 1271–1279

[16] Parniani, M., Vanouni, M.: 'A fast local index for online estimation of closeness to loadability limit', *IEEE Trans. Power Syst.*, 2010, **25**, (1), pp. 584–585

[17] Milošević, B., Begović, M.: 'Voltage-stability protection and control using a wide-area network of phasor measurements', *IEEE Trans. Power Syst.*, 2003, **18**, (1), pp. 121–127

[18] Wang, Z., Cui, B., Wang, J.: 'A necessary condition for power flow insolvability in power distribution systems with distributed generators', *IEEE Trans. Power Syst.*, 2017, **32**, (2), pp. 1440–1450

[19] Aolaritei, L., Bolognani, S., Dörfler, F.: 'A distributed voltage stability margin for power distribution networks', arXiv: 1612.00207 [math.OC]

[20] Xu, W., Pordanjani, I.R., Wang, Y., *et al.*: 'A network decoupling transform for phasor data based voltage stability analysis and monitoring', *IEEE Trans. Smart Grid*, 2012, **3**, (1), pp. 261–270

[21] Pordanjani, I.R., Wang, Y., Xu, W.: 'Identification of critical components for voltage stability assessment using channel components transform', *IEEE Trans. Smart Grid*, 2013, **4**, (2), pp. 1122–1132

[22] Liu, J.-H., Chu, C.-C.: 'Wide-area measurement-based voltage stability indicators by modified coupled single-port models', *IEEE Trans. Power Syst.*, 2014, **29**, (2), pp. 756–764

[23] Wang, Y., Wang, C., Lin, F., *et al.*: 'Incorporating generator equivalent model into voltage stability analysis', *IEEE Trans. Power Syst.*, 2013, **28**, (4), pp. 4857–4866

[24] Dobson, I.: 'Observation on the geometry of saddle node bifurcation and voltage collapse in electric power systems', *IEEE Trans. Circuit Syst. I*, 1992, **39**, (3), pp. 240–243

[25] Kuznetsov, Y.: '*Elements of applied bifurcation theory*' (Springer, New York, 1998)

[26] Van Cutsem, T., Vournas, C.: '*Voltage stability of electric power systems*' (Springer, New York, NY, USA, 2008)

[27] Vournas, C.: 'Maximum power transfer in the presence of network resistance', *IEEE Trans. Power Syst.*, 2015, **30**, (5), pp. 2826–2827

[28] Reinhard, K.E., Sauer, P.W., Domínguez-García, A.D.: 'On computing power system steady-state stability using synchrophasor data'. Proc. 46th Hawaii Int. Conf. System Sciences, Maui, HI, USA, 7–10 January 2013, pp. 1–7

[29] Bolognani, S., Carli, R., Todescato, M.: 'State estimation in power distribution networks with poorly synchronized measurements'. IEEE Conf. on Decision and Control, Los Angeles, CA, USA, December 2014, pp. 2579–2584

[30] Gao, B., Morison, G.K., Kundur, P.: 'Voltage stability evaluation using modal analysis', *IEEE Trans. Power Syst.*, 1992, **7**, (4), pp. 1529–1542

[31] Zimmerman, R.D., Murillo-Sánchez, C.E., Thomas, R.J.: 'MATPOWER: steady-state operations, planning and analysis tools for power systems research and education', *IEEE Trans. Power Syst.*, 2011, **26**, (1), pp. 12–19

[32] Kundur, P.: '*Power system stability and control*' (McGraw-Hill, New York, 1994)

8 Appendix

8.1 Derivation of modified equivalent voltage $|E_{\text{eq},j}|$

The sensitivity of F with respect to the magnitude of load voltage $|V_j|$ is

$$\begin{aligned}\frac{\partial F}{\partial |V_j|} &= 4|V_j|^3 - 2|V_j|(|E_{\text{eq},j}|^2 - 2(R_{\text{eq},j}P_j + X_{\text{eq},j}Q_j)) \\ &= 4|V_j|^3 - 2|V_j|(|V_j|^2 + |V_{\text{line}}|^2) \\ &= 4|V_j|^3 - 2|V_j|(2|V_j|^2 + |E_{\text{eq},j}|^2 - 2|E_{\text{eq},j}||V_j|\cos(\theta_e - \\ &= -2|V_j||E_{\text{eq},j}|(|E_{\text{eq},j}| - 2|V_j|\cos(\theta_e - \theta)).\end{aligned}$$

The sensitivity of F with respect to real load power P_j is

$$\begin{aligned}\frac{\partial F}{\partial P_j} &= 2|V_j|^2(R_{\text{eq},j} + qX_{\text{eq},j}) + (R_{\text{eq},j}^2 + X_{\text{eq},j}^2)(2P_j + 2q^2P_j) \\ &= \frac{2|V_j|^2}{P_j}(R_{\text{eq},j}P_j + X_{\text{eq},j}Q_j) + \frac{2}{P_j}|Z_{\text{eq},j}|^2|S_j|^2 \\ &= \frac{2|V_j|^2}{P_j}(R_{\text{eq},j}P_j + X_{\text{eq},j}Q_j) + \frac{2}{P_j}|V_{\text{line}}|^2|V_j|^2 \\ &= \frac{2|V_j|^2}{P_j}(R_{\text{eq},j}P_j + X_{\text{eq},j}Q_j + |V_{\text{line}}|^2) \\ &= \frac{2|V_j|^2}{P_j}\left(\frac{|E_{\text{eq},j}|^2 - |V_j|^2 - |V_{\text{line}}|^2}{2} + |V_{\text{line}}|^2\right) \\ &= \frac{|V_j|^2}{P_j}(|E_{\text{eq},j}|^2 - |V_j|^2 - |V_{\text{line}}|^2) \\ &= \frac{2|V_j|^2|E_{\text{eq},j}|}{P_j}(|E_{\text{eq},j}| - |V_j|\cos(\theta_e - \theta)).\end{aligned}$$

Substitute the two sensitivities into (33)

© The Institution of Engineering and Technology 2017

$$
\begin{aligned}
0 &= \frac{\partial F}{\partial |V_j|} + \gamma \frac{\partial F}{\partial |V_j|} \\
&= -E_{\text{eq},j} + 2|V_j|\cos(\theta_e - \theta) + \frac{\gamma |V_j|}{P_j}(|E_{\text{eq},j}| - |V_j|\cos(\theta_e - \\
&= \left(\frac{\gamma |V_j|}{P_j} - 1\right)|E_{\text{eq},j}| + \left(2 - \frac{\gamma |V_j|}{P_j}\right)|V_j|\cos(\theta_e - \theta).
\end{aligned}
$$

Therefore we have

$$
|E_{\text{eq},j}| = \frac{2 - \gamma |V_j|/P_j}{1 - \gamma |V_j|/P_j}|V_j|\cos(\theta_e - \theta).
$$

© The Institution of Engineering and Technology 2017